Research on the MIMO short-range imaging mechanism of millimeter wave for fast and accurate reconstruction

YU Yang[1,2], YOU Yan[2], CHEN Xu-Dong[3], QIAO Ling-Bo[2], ZHAO Zi-Ran[1,2*]

（1. Department of Engineering Physics, Tsinghua University, Beijing 100084, China;
2. National Engineering Laboratory for Dangerous Articles and Explosives Detection Technologies, Tsinghua University, Beijing 100084, China;
3. Department of Electrical and Computer Engineering, National University of Singapore, Singapore 117583, Singapore）

Abstract：Millimeter-wave (MMW) imaging is of interest as it has played an essential role in personal surveillance. The existing MMW short-range imaging mechanisms in personal surveillance can be mainly divided into SISO and MIMO. The SISO mechanism can achieve fast and accurate imaging. However, as the operating frequency increases, the number of antennas required increases rapidly, and the antenna spacing decreases, which not only causes an increase in system cost, but also makes it difficult to suppress antenna coupling. Although the MIMO mechanism reduces the number of antennas required for imaging and increases the antenna spacing, it is currently unable to achieve rapid and accurate reconstruction comparable to the SISO mechanism. In this paper, a MIMO short-range imaging mechanism has been proposed, which is well-suitable for fast and accurate reconstruction, and the applicable conditions of the mechanism were given quantitatively. Unlike the traditional MIMO short-range imaging mechanism, the proposed MIMO imaging mechanism satisfies the principle of equivalent phase center (EPC) in short-range imaging by ingeniously designing MIMO sub-arrays. Therefore, it can directly use various accurate and fast imaging algorithms developed for SISO mechanism to reconstruct images, such as range migration algorithm (RMA). It means that the algorithm has the advantages of both SISO mechanism and MIMO mechanism. The demonstrations in E-band show that the proposed MIMO mechanism exhibits the same level of imaging quality and reconstruction speed as SISO mechanism in short-range imaging, but the antenna utilization rate and the antenna spacing can be increased by more than 4 times. When compared with the traditional MIMO imaging mechanism, the proposed MIMO mechanism not only has better imaging quality but also greatly improves the reconstruction speed, which is nearly 200,000 times faster than the traditional MIMO mechanism in a typical imaging scene of 1m×1m×0. 2m volume with a voxel size of 1. 85 mm^3. Both simulation and experimental results verify the effectiveness of the proposed MIMO mechanism.

Key words：millimeter wave, MIMO, short-range imaging, fast and accurate imaging algorithm

可快速精确重建的毫米波 MIMO 近距离成像机制研究

于 洋[1,2]，游 燕[2]，陈旭东[3]，乔灵博[2]，赵自然[1,2*]
（1. 清华大学 工程物理系,北京 100084;
2. 清华大学 危爆物品扫描探测国家工程实验室,北京 100084;
3. 新加坡国立大学 电子与计算机工程系,117583 新加坡）

摘要：毫米波成像在人体安检领域发挥了重要作用,引起了人们的广泛关注。现有的毫米波近场人体安检成像机制主要分为 SISO 和 MIMO 两种。SISO 机制可实现快速精确成像,然而随着工作频率的升高,其所需天线数目迅速增长、天线间隔下降,不仅造成了系统成本提升,还使得天线耦合难以被抑制。MIMO 机制虽然降低

YU Yang *et al*：Research on the MIMO short-range imaging mechanism of millimeter wave for fast and accurate reconstruction

5 期

639

了成像所需的天线数目、增大了天线间隔，但目前无法实现类似SISO机制的快速精确重建。提出了一种可快速精确重建的MIMO近距离成像机制，定量给出了该机制的适用条件。与传统MIMO近距离成像机制不同，该MIMO近距离成像机制通过巧妙地设计MIMO子阵列，使其在近场成像中满足等效相位中心原理。因此它能够直接使用诸如距离迁徙算法（range migration algorithm，RMA）等各种基于SISO机制开发的精确且快速的成像算法去重建图像，兼顾了SISO机制和MIMO机制的优势。E波段的示例表明，在近场毫米波成像中，该MIMO机制与SISO机制具有同等水平的成像质量和成像速度，但相较于SISO机制，该MIMO机制的天线利用率、天线间隔可提升4倍以上。与传统MIMO成像机制相比，该MIMO成像机制不但有更好的成像质量，而且其重建速度大幅提升，在一个成像区域为 1 m×1 m×0.2 m，体素尺寸为 1.85 mm³ 的典型成像场景中，比传统MIMO成像机制快近 200,000 倍。仿真和实验结果验证了该成像机制的有效性。

关　键　词：毫米波；MIMO；近距离成像；快速精确成像算法

Introduction

Due to the characteristics of nonionizing radiation, high resolution and good penetrability, active MMW imaging applied to personnel surveillance has been extensively studied over the past decades [1-4]. The most classical MMW imaging mechanism is what we called SISO in which transmitting antenna（T）and receiving antenna（R）are co-located, and a two-dimensional（2D）aperture is achieved by scanning electrically or mechanically [5-6]. Researchers have developed various fast imaging algorithms for SISO mechanism in the past decades [1-2,7-9]. Range migration algorithm（RMA）is one of them. And this FFT-based imaging method is thought to be a standard imaging algorithm for SISO mechanism because of both high accuracy and rapid computation speed. When imaging a volume that consists of $N \times N \times N$ points, the computational complexity of RMA is $O(N^3 \log_2 N)$. Combined with broadband signal and RMA, SISO imaging system can achieve good 3D imaging results in short-range and has been widely used in personnel surveillance [9-11]. However, SISO setup requires that the spacing of transceivers is less than half of wavelength because of the limitation of Nyquist criterion. Since spatial resolution has a consistent dependence regarding the frequency and the aperture size, to improve the resolution of images, higher central frequency and larger aperture must be used, making the number of antennas increases rapidly. And more antennas contribute to the systems cost and complexity arising. Besides, the decrease of the interval between transceivers has an adverse effect on antenna design and coupling suppression.

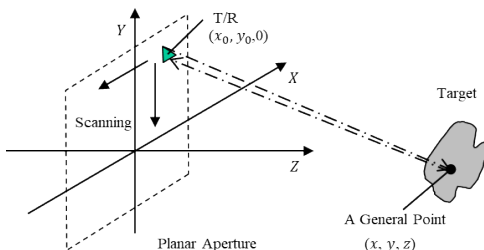Therefore, some researchers have set their sights on

Fig. 1　Schematic diagram of SISO imaging mechanism
图 1　SISO 成像体制原理示意图

the mechanism of MIMO in which transmitting and receiving antennas are not co-located. MIMO antenna array operates sequentially or simultaneously, when one transmitting antenna emits signal, multiple receiving antennas receive the echo signal. Compared with the SISO imaging system, the MIMO imaging system requires fewer antennas, has faster scanning speed, and the antennas can be sparsely arranged. We noticed that there are some research focusing on MIMO array topology design [12-16]. However, MIMO mechanism faces a main challenge of fast image reconstruction. Most of researches usually use the back-projection algorithm（BPA）to reconstruct images. While BPA is accurate and suitable for any MIMO array configuration, its computational complexity is too tremendous. Especially in 3D cases, the computational complexity of BPA can reach $O(N^5)$. RMA has long been used efficiently in SISO setup but cannot be directly used in MIMO configuration. Recently, another FFT-based imaging algorithm for MIMO configuration was proposed in Ref.［17］, but as the paper shows, when compared with traditional RMA used in SISO, the speed of image reconstruction is still slow, and the computational complexity of the algorithm is $O(N^4 \log_2 N)$.

In this study, a MIMO short-range imaging mechanism of MMW for fast and accurate reconstruction is presented. The proposed MIMO imaging mechanism adopts a mechanical scanning MIMO linear array in order to balance the system cost and scanning speed. Through the sparse design of antenna array and control technology, the data acquisition speed and the utilization rate of antenna can be greatly improved. Meanwhile, the antennas in the MIMO array are arranged sparsely, which helps to couple suppression and hardware complexity reduction. More importantly, the MIMO mechanism could use accurate and fast imaging algorithms developed for SISO mechanism, such as RMA, to reconstruct images, which significantly improves the speed of reconstruction. It must be noted that RMA is just one type of fast imaging algorithms, and we choose it to verify the effectiveness of our mechanism for its generality. In essence, the proposed MIMO mechanism is suitable for a variety of fast imaging algorithms developed based on SISO mechanism, such as phase shift migration algorithm（PSMA）[7], range resolution enhancement algorithm（RREA）[8].

The applicability of the proposed MIMO mechanism will not be affected by the change of algorithm.

1 Method

1. 1 Background: SISO imaging mechanism

Before discussing the MIMO mechanism, we first review the SISO imaging mechanism and its image reconstruction algorithms. As shown in Fig. 1, transmitting and receiving antennas are co-located and a 2D aperture are formed to build 3D images by electrical or mechanical scanning technology. And the 2D aperture is located on the plane at $Z=0$ in Cartesian coordination. The targets are located in the area of $Z>0$, and under Born approximation [18] and ignore the propagation attenuation, then the scattering data collected by 2D-SISO antenna aperture can be expressed as:

$$s(x_0,y_0,k) = \iiint f(x,y,z)\exp(-2jkr)dxdydz, \quad (1)$$

where $r = \sqrt{(x_0 - x)^2 + (y_0 - y)^2 + z^2}$ represents the distance between the antenna at $(x_0, y_0, 0)$ with the target at (x, y, z). k represents the wavenumber, and $f(x,y,z)$ is the reflectivity distribution of the target.

Typically, the antennas are evenly distributed in 2D aperture. According to the sampling requirement, the interval between antennas should satisfy the Nyquist criterion [19]:

$$\Delta x \leqslant \frac{\lambda_{\min}}{2} \frac{\sqrt{\frac{(L_x + D_x)^2}{4} + Z_0{}^2}}{L_x + D_x},$$

$$\Delta y \leqslant \frac{\lambda_{\min}}{2} \frac{\sqrt{\frac{(L_y + D_y)^2}{4} + Z_0{}^2}}{L_y + D_y}, \quad (2)$$

where Δx and Δy are the sampling step in the cross-range plane, $\lambda_{\min}$ represents the shortest wavelength within frequency band. L_x and L_y are the width and height of antenna array. D_x and D_y are the width and height of imaging domain. Z_0 represents the front surface of the target on the Z-axis. However, due to the beam-width of antenna is limited, usually setting the internal as $\lambda_{\min}/2$ is sufficient. Because the sampling of antenna is uniform, so RMA can be used. The imaging process can be described as Ref. [1]:

$$f(x,y,z) = FT_{3D}^{-1}[FT_{2D}[s(x_0,y_0,k)] \\ \exp(-jZ\sqrt{k^2 - k_x^2 - k_y^2})] \quad , \quad (3)$$

FT_{3D}^{-1} and FT_{2D} represent the 3D Fourier inverse converter and 2D Fourier transform operator, respectively. k_x and k_y stand for the spatial wavenumbers in x- and y- directions, respectively.

1. 2 Dimension Reduction for MIMO imaging mechanism

For MIMO imaging mechanism, transmitting and receiving antennas are not co-located. The process of scattering data acquirement can be written as:

$$s(x_T,y_T,x_R,y_R,k) = \iiint f(x,y,z)\exp(-jkr_T)\exp(-jkr_R)dxdydz, \quad (4)$$

where r_T stands for the distance between the transmitter at $(x_T, y_T, 0)$ and the target at (x, y, z). r_R the represents the distance between receiver at $(x_R, y_R, 0)$ and target at (x, y, z).

Obviously, the scattering data set is a 5-D matrix in MIMO imaging system. To reconstruct a 3-D image by RMA, the operation of dimension reduction must be done. Equivalent phase center (EPC) principle is a simple and effective method for spatial dimension reduction [20]. Based on the principle, each pair of transmitter-receiver form an EPC, which lies on the midpoint of the two antennas. Therefore, in Cartesian coordination, the coordinate of EPC can be expressed as:

$$x_c = \frac{x_T + x_R}{2}, y_c = \frac{y_T + y_R}{2} \quad , \quad (5)$$

Then, the 5D data $s(x_T, y_T, x_R, y_R, k)$ is rewritten as a 3-D data $s(x_C, y_C, k)$. Hence, RMA can be used, a 3-D image can be formed with the following expression:

$$f(x,y,z) = FT_{3D}^{-1}[FT_{2D}[s(x_C,y_C,k)] \\ \exp(-jZ\sqrt{k^2 - k_x^2 - k_y^2})] \quad , \quad (6)$$

Nevertheless, the EPC principle is valid only under the far-field condition, i. e., the imaging distance is much larger than the size of MIMO array, which can be expressed as Rayleigh's far-field criterion [21]:

$$R \geqslant \frac{2L^2}{\lambda_{\min}}, \quad (7)$$

where R is the distance between target with MIMO array, L represents the length of MIMO array. However, the condition fails to be met in traditional MIMO shot-range imaging mechanism. For example, the imaging area of MMW human security inspection system is about 1 m×2 m and the operating wavelength usually less than 0.01m. However, the maximum detection distance of the system is usually under 1 meter because of the low power of sources. In this paper, a MIMO mechanism that uses several sub-arrays is proposed, which can use various accurate and fast imaging algorithms developed for SISO mechanism to reconstruct images without obvious image degradation.

1. 3 MIMO linear array topology design

The MIMO linear array adopted by the presented MIMO mechanism is depicted as Fig. 2 ($N_1 = 2, N_2 = 3$ is shown). Array 1 has N_1 elements over unit cell length D for spacing of D/N_1. Array 2 has N_2 elements over unit cell length D for spacing D/N_2. We assume $N_1 < N_2$ and no common factor is shared between N_1 and N_2 for sampling uniformly. Usually, array 1 are set as transmitter array and array 2 are set as receiver array. To satisfy the requirement of far-field condition, when one transmitter emits signal, only the receivers whose separation with the transmitter is less than or equal to D are used to receive the echo signal. The largest separation D should meet the formula:

$$D \leqslant \sqrt{\frac{R\lambda_{\min}}{2}} \quad , \quad (8)$$

As shown in the Fig. 2, except for those elements

in the end cells，each element in array 1 forms $2N_2$ sampling data. To meet the requirement of uniform sampling，only EPCs whose position $\geq D/2$ are adopted in left end cell and only EPCs whose position $\leq D/2$ are adopted in right end cell.
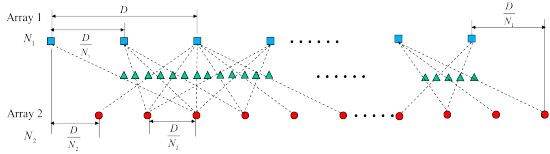

Fig. 2　Diagram of MIMO linear array configuration adopted by the proposed new MIMO mechanism
图 2　新型 MIMO 体制线性天线阵列配置示意图

We define the number of cells as N_c, then the number of elements in array 1 and array 2 can be written as N_1N_c, N_2N_c. The interval of EPC is $D/(2N_1N_2)$ and length of EPC array can be expressed as：

$$L_E = (N_c - 1)D \qquad . \quad (9)$$

Hence，compared with SISO array，the antenna utilization rate in this MIMO array can be expressed as：

$$\eta = \frac{2N_1N_2(N_c - 1) + 1}{(N_1 + N_2)N_c} \qquad . \quad (10)$$

Since the interval of EPC usually was set as $\lambda_{\min}/2$, then Eq.（8）can be conducted as：

$$N_1N_2 \leq \sqrt{\frac{R}{2\lambda_{\min}}} \qquad . \quad (11)$$

Formula（11）quantitively gives the applicable condition of the proposed MIMO mechanism. Furthermore，（11）indicates that the utilization rate of antenna in the MIMO array can be improved by the increase of imaging distance and frequency. It means that the advantages of the MIMO array will be more obvious when working at high frequency.

In addition，the traditional MIMO imaging mechanism in Ref.［22］is introduced for comparation. As shown in Fig. 3，the traditional MIMO imaging mechanism can use less antennas to form same number of EPCs when compared with our MIMO imaging mechanism. However，those fast and accurate imaging algorithms，which are developed based on SISO mechanism，are not applicable for traditional MIMO linear arrays. This will be demonstrated in the next section.
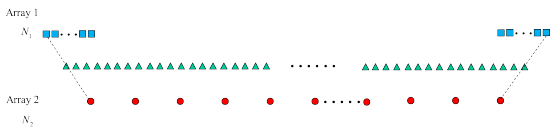

Fig. 3　Diagram of MIMO linear array configuration adopted by the traditional MIMO mechanism
图 3　传统 MIMO 体制线性天线阵列配置示意图

2　Verification process

In this section，we did both simulations and experiments to verify the MIMO imaging mechanism. As shown

in Fig. 4，a 2D test pattern is set as the imaging target in numerical simulations. And a 3D mannequin whose material was set as perfect electrical conductor（PEC）serves as target in electromagnetic simulations.
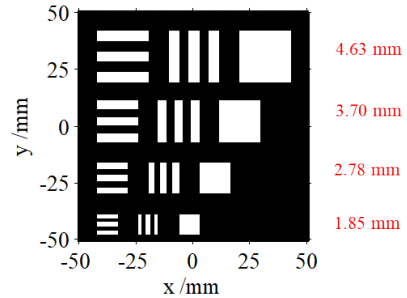

Fig. 4　Drawing of resolution chart
图 4　分辨率测试板示意图

2. 1　Numerical Simulations

The adopted MMW source is 70~82 GHz with a sampling interval of 0. 25 GHz. The imaging range is 0. 3 meter and the holographic data are obtained by（4）. Based on the design method in section II，we design a set of MIMO linear arrays with different N_1：N_2：N_c but nearly identical EPC array in order to testify the effectiveness of the proposed MIMO imaging mechanism. From Eq.（11），we can deduce that $N_1N_2 \leq 6.36$. So, the N_1：N_2：N_c of those MIMO arrays are set as 1：4：69, 2：3：47, 1：8：35, 1：10：28. And the traditional MIMO imaging mechanism that adopts 20 transmitters and 27 receivers is used for comparation. Every MIMO linear array can form a 1-meter-long and 0. 5-$\lambda_{\min}$-spaced EPC linear array. Similarly，the classical SISO mechanism with a linear array whose elements located at the EPC of the MIMO array is also introduced for comparison. All linear arrays are uniformly moved in vertical direction with 0. 5$\lambda_{\min}$ step to form a 1 m×1 m scanning aperture.
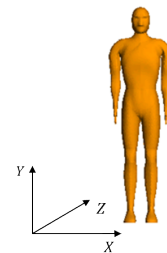

Fig. 5　Illustration of mannequin
图 5　人体模特示意图

Fig. 6 shows the maximum value projection of the imaging results of the resolution chart. Not surprisingly，traditional MIMO array leads to unfocused images when imaging with RMA. In addition，the imaging quality of traditional MIMO array with BPA is not satisfactory because overly spare MIMO array brings obvious artifact in horizontal direction. And as shown in Fig.（a）and（e），by imaging with RMA，the reconstructed images of the 2：
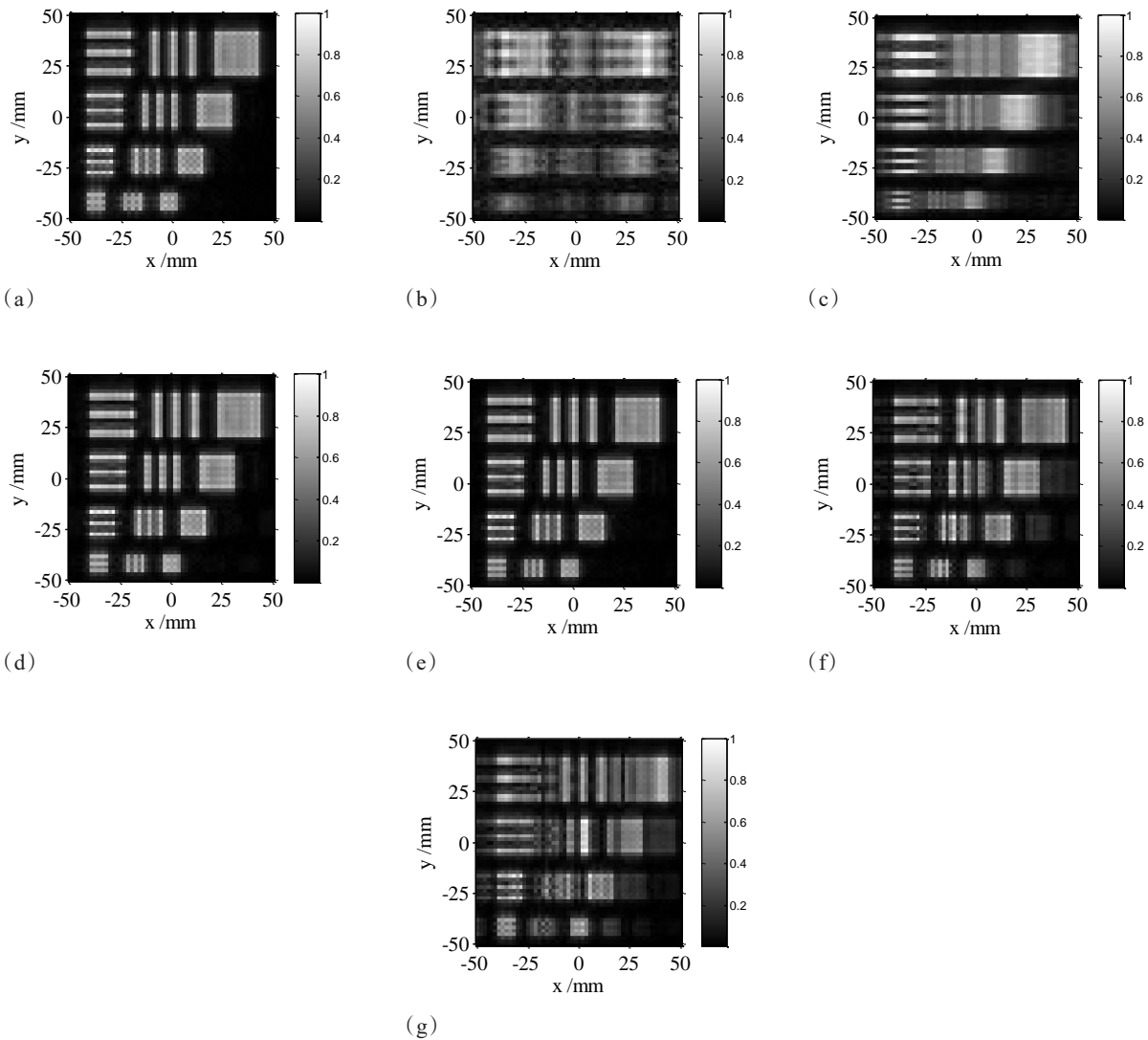
Fig. 6 Reconstructed images (maximum projection) of resolution chart via numerical simulattons (a) SISO array with RMA (b) traditional MIMO array with RMA (c) traditional MIMO array with BPA (d) 1:4:69 MIMO array with RMA (e) 2:3:47 MIMO array with RMA (f) 1:8:35 MIMO array with RMA (g) 1:10:28 MIMO array with RMA

图 6 分辨率测试板数值仿真成像结果 (a) 采用RMA的SISO阵列 (b) 采用RMA的传统MIMO阵列 (c) 采用BPA的传统MIMO阵列 (d)采用RMA的 1:4:69 MIMO阵列 (e) 采用RMA的 2:3:47 MIMO阵列 (f) 采用RMA的 1:8:35 MIMO阵列 (g) 采用RMA的 1:10:28 MIMO阵列

3：47 MIMO array and SISO array are of high consistency. However, the total number of antennas in the 2：3：47 MIMO drops by more than 78.7% and the interval between antennas in the 2：3：47 MIMO array increases fourfold when compared with the SISO array. Comparing Fig. 6(a), (d), (e), (f), and (g), one can see that the lateral resolution of MIMO arrays is equal to that of the SISO array while $N_1N_2 \leqslant 6.36$. However, when it comes to $N_1N_2 > 6.36$, the lateral resolution and imaging quality of MIMO array deteriorate rapidly with the increase of N_1N_2. This is because the EPC principle is no longer valid and the phase errors caused by it increase dramatically with the increase of N_1N_2. The simulation results intuitively demonstrate the effectiveness of the proposed MIMO imaging mechanism and its applicational condition.

To quantitatively compare the imaging quality of different imaging mechanism, we adopt the index of peak side-lobe ratio (PSLR). An ideal scattering point that is located at $(0, 0, 0.3)$ serves as the imaging target. After imaging, 3D imaging result is projected in x-y plane, then the PSFs in the array direction are plotted in Fig. 7. Table 1 lists the antenna utilization rate, the PSLR corresponding Fig. 7 and the computational time of those arrays for imaging a $1m×1m×0.2m$ volume with a voxel size of $1.85mm^3$. The data are obtained on a PC with Intel i7-7560U platform using MATLAB codes and no parallel computing or GPU acceleration techniques are used.

From Fig. 7 and Table 1, we see that the shape of PSF and the PSLR of the proposed MIMO imaging mechanism are very similar to those of the classical SISO mech-

anism when $N_1 N_2 \leqslant 6.36$. As expected，when $N_1 N_2 > 6.36$，the differences between the proposed MIMO mechanism with the SISO mechanism expand rapidly as the increase of $N_1 N_2$. It demonstrates the effectiveness of Eq. （11）. In addition，the PSLR of the proposed MIMO mechanism is much lower than traditional MIMO mechanism when $N_1 N_2 \leqslant 6.36$. It explains why our MIMO mechanism has better imaging performance.

2. 2　Electromagnetic Simulations

We used the electromagnetic simulation software FEKO with the Physical-Optics（PO）method to obtain the results of electromagnetic simulations. The mannequin is placed between Z=0. 15 m and Z=0. 35 m. We use MMW between 70-82 GHz with an interval of 0. 25 GHz to illuminate the target. One electric dipole is used as an antenna. Similarly，a 1-meter-long MIMO array and the SISO array whose elements located at the equivalent phase center are chosen for comparation. Based on Eq. （11），we conclude that $N_1 N_2 \leqslant 4.5$. To verify the accuracy of the proposed MIMO mechanism more comprehensively，$N_1 : N_2 : N_c$ is set as 1：4：69. By evenly moving linear array along the vertical direction，a 1 m×1 m scanning aperture is formed to reconstruct images.

Fig. 8 is the maximum projection of imaging results of the mannequin. We can see that the difference between Fig. 8（a）with Fig. 8（b）is very minor. Fig. 9 shows the PSFs of the two mechanisms. And the ideal scattering point is located at（0，0，0. 25）. One can see that the PSF of the proposed MIMO mechanism is almost coincided with that of the SISO mechanism.

The computational time of the two mechanisms for imaging a 1m×1m×0. 2 m volume with an interval of 1. 85 mm and the PSLR corresponding Fig. 9 are listed in Table 2. The computational time and PSLR of the proposed MIMO imaging mechanism are approximately the same with those of SISO mechanism. The electromagnetic simulation results further verify the effectiveness of our MIMO imaging mechanism.

2. 3　Experiment Results

In this section，the experiments are designed to cross-validate with the simulations. As shown in Fig. 10，a vertical scanning equipment is used to move the MIMO linear array. The MIMO linear array and MMW source are set up with the same parameters as electromagnetic simulations. For the configure of SISO array imaging system，the schematic diagram and photograph are shown in Fig . 11. We just use one pair of transmitter-receiver in the above MIMO array to form a SISO channel and the target is moved by the 2D scanner.

A metal resolution test chart，which is very similar to that in numerical simulations，is used to test the performance of the MIMO imaging system and the SISO imaging system. The resolution test chart is placed 0. 4 m in front of the scanning aperture and the scanning aperture is set as 1m×1m with a 1. 85 mm interval in both the MIMO imaging system and the SISO imaging system. Fig. 12 shows the imaging results of the resolution test chart. We can see that the MIMO imaging system and the SISO imaging system has a comparable lateral resolution，which is better than 2. 8 mm but worse than 2. 5 mm. However，the image reconstructed by the SISO imaging system has more speckles noise than the MIMO imaging system. This is because in the MIMO imaging system，when one transmitter emits signal，multiple receivers at different positions simultaneously receive the echo signal to form multiple different observation angles. As mentioned in reference[23]，the observation from multiple different angles will reduce speckles noise.

Since the parameter configurations are the same with electromagnetic simulations，and the size of data and the number of antennas are the same. Hence，the computational time and antenna utilization rate of the proposed MIMO imaging mechanism and the SISO imaging mechanism are also the same with the results in Table 2，and we will not repeat it here.

In order to further test the performance of the proposed MIMO imaging mechanism in practical applica-

Table 1　Comparison on Antenna utilization rate, computational time and PSLR of different Imaging mechanisms or arrays, in numerical simulations
表1　数值仿真中不同成像体制或不同阵列的天线利用率、计算时间及峰值旁瓣比

Array	Algorithm	Antenna utilization rate	Computational time（s）	PSLR（dB）
SISO	RMA	0. 5	39. 37	−32. 69
Traditional MIMO	BPA	11. 49	7495040. 27	−19. 83
1：4：69 MIMO	RMA	1. 58	39. 28	−32. 11
2：3：47 MIMO	RMA	2. 35	39. 31	−30. 36
1：8：35 MIMO	RMA	1. 73	39. 89	−19. 24
1：10：28 MIMO	RMA	1. 76	39. 30	−13. 01

Table 2　Comparison on Antenna utilization rate, computational time and PSLR of different mechanism in electromagnetic simulations.
表2　电磁仿真中不同成像体制的天线利用率、计算时间及峰值旁瓣比

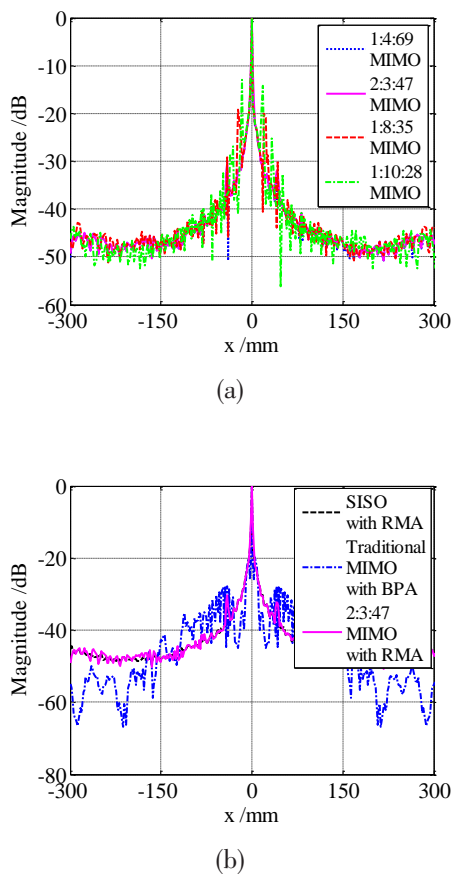| Array	Algorithm	Antenna utilization rate	Computational time（s）	PSLR（dB）
SISO	RMA	0. 5	39. 20	−30. 33
1：4：69 MIMO	RMA	1. 58	39. 39	−30. 35

(a)

(b)

Fig. 7 PSFs of different arrays or different mechanisms for numerical simulations. (a) different arrays. (b) different mechanisms
图 7 不同成像体制或不同阵列的点扩散函数数值仿真结果 (a) 不同阵列 (b)不同成像体制 Besides, by imaging with RMA, the computational time of proposed MIMO mechanism is approximately same with that of SISO mechanism. Compared with the traditional MIMO mechanism, the proposed MIMO mechanism not only gets better imaging performance but also faster reconstruction speed. The computational time of proposed MIMO mechanism is just about 0.00052% that of the traditional MIMO mechanism. It verifies the superiority of the proposed MIMO mechanism.

tion，we choose a child mannequin as a 3D target to represent the subjects most at risk. Moreover，detection of a child is harder than an adult for its smaller size. The child mannequin is located in 0.2~0.4 m in front of scanning aperture and the scan length along vertical direction is set to 1m and the interval is 1.85 mm. The photograph and reconstructed image of the child mannequin are shown in Fig. 13. It can be observed that the details of the child mannequin are well recognized. Besides，we can see that there are bright spots in the shoulders and left leg of the child mannequin，which are caused by the metal fasteners inside the mannequin. This also proves the penetrability of MMW used in the MIMO imaging system.

From the above imaging results，we see that the experimental results are highly consistent with the simulation results. For the proposed MIMO imaging mecha-
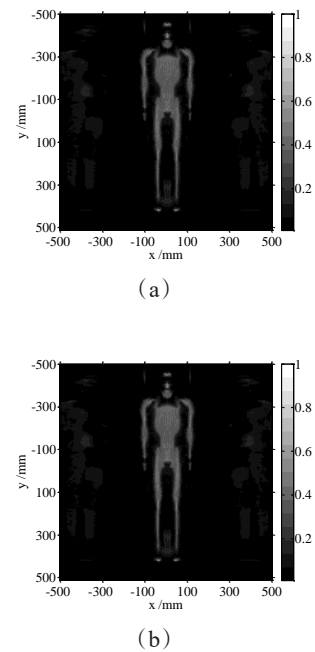

(a)

(b)

Fig. 8 Reconstructed images (maximum projection) of mannequin via electromagnetic simulations. (a) SISO array with RMA. (b)1:4:69 MIMO array with RMA
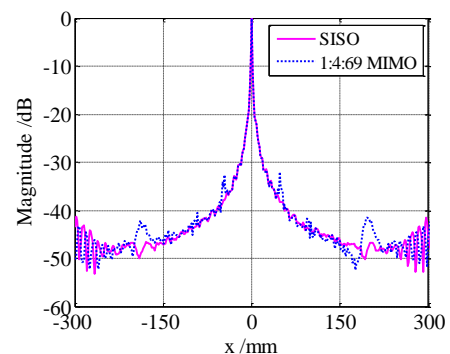图 8 人体模特电磁仿真成像结果 (a) 采用RMA的SISO阵列 (b)采用RMA的1:4:69 MIMO阵列

Fig. 9 PSFs of different mechanisms for electromagnetic simulation
图 9 不同成像体制的点扩散函数电磁仿真结果

nism，both 2D and 3D targets can be completely focused and accurately imaged by using RMA，which means the proposed MIMO mechanism is suitable for fast imaging algorithms developed for SISO mechanism. In addition，compared with the SISO imaging mechanism，the proposed MIMO imaging mechanism has a comparable imaging resolution，but higher antenna utilization and lower speckles noise due to the advantages of MIMO mechanism. In other words，the proposed MIMO imaging mechanism has the advantages of both SISO mechanism and MIMO mechanism.

3 Conclusion

A MIMO short-range imaging mechanism of MMW that can achieve fast and accurate reconstruction is pre-

YU Yang *et al*：Research on the MIMO short-range imaging mechanism of millimeter wave for fast and accurate reconstruction

5 期

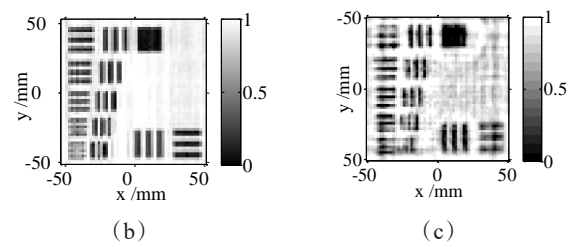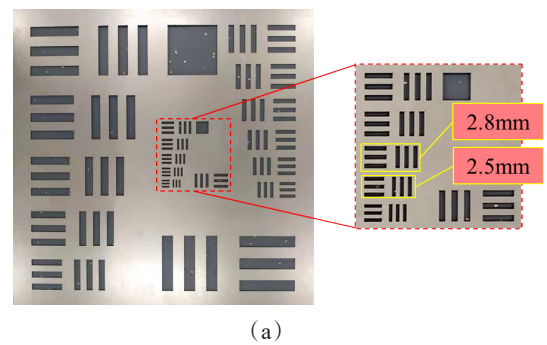645

Fig. 10　Photograph of vertical scanner
图 10　垂直扫描仪光学图像

（a）

Fig. 11　Schematic diagram and photograph of SISO imaging system (a) Schematic diagram (b) Photograph.
图 11　SISO 成像系统原理示意图及光学图像 (a) 原理示意图 (b)光学图像

sented. The applicable conditions of the mechanism are given quantitatively. The feasibility of the method is veri-
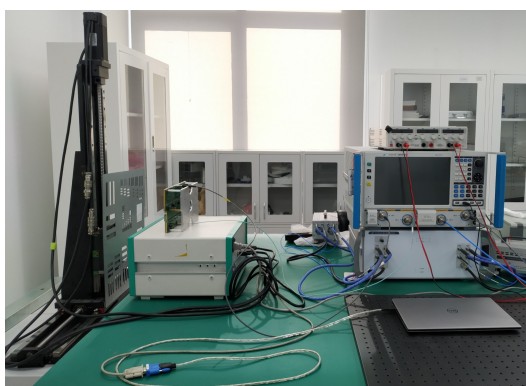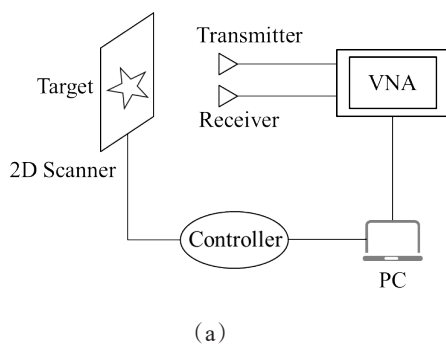

Fig. 12　Measurement of the resolution test chart (a) Photograph (b) Reconstructed image of 1:4:69 MIMO array with RMA (c) Reconstructed image of SISO array with RMA
图 12　分辨率测试板测量结果 (a) 光学图片 (b)采用 RMA 的 1:4:69 MIMO 阵列重建结果 (c) 采用 RMA 的 SISO 阵列重建结果
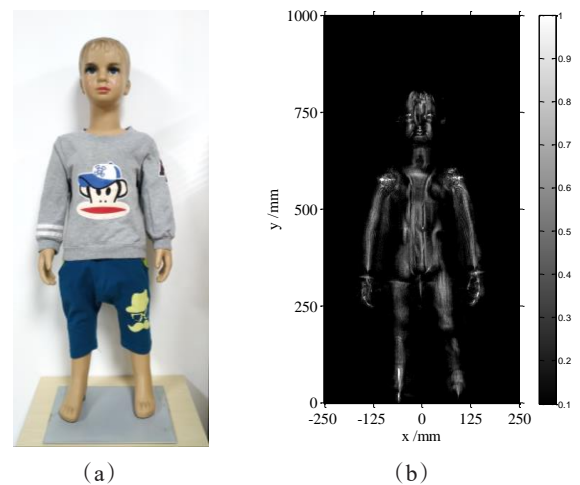

Fig. 13　Measurement of the child mannequin (a) Photograph (b) Reconstructed image of 1:4:69 MIMO array with RMA
图 13　儿童人体模特测量结果 (a) 光学图片 (b)采用 RMA 的 1:4:69 MIMO 阵列重建结果

fied by simulations and experiments. The results demonstrate that the MIMO imaging mechanism presented in the paper is suitable for RMA and the applicable conditions of the mechanism are effective. When imaging with RMA，the quality and the computational time of reconstructed images formed by our MIMO mechanism are similar to those formed by the SISO mechanism but the antenna utilization rate and antenna spacing are much better than traditional MIMO mechanism. Compared with

the traditional MIMO imaging mechanism, although the proposed MIMO mechanism requires more antennas, it can achieve higher imaging quality and its applicability to various fast imaging algorithms greatly improves the imaging speed of the MIMO system.

Reference

[1] Sheen D M, McMakin D L, Hall T E. Three-dimensional millimeter-wave imaging for concealed weapon detection[J]. *IEEE Transactions on microwave theory and techniques*, 2001, **49**(9): 1581-1592.

[2] Qiao L, Wang Y, Zhao Z, *et al*. Exact reconstruction for near-field three-dimensional planar millimeter-wave holographic imaging[J]. *Journal of Infrared*, Millimeter, and Terahertz Waves, 2015, **36**(12): 1221-1236.

[3] Ahmed S S. Personnel screening with advanced multistatic imaging technology[C]//Passive and Active Millimeter-Wave Imaging XVI. International Society for Optics and Photonics, 2013, **8715**: 87150B.

[4] Wang Z, Qiao L, Wang Y, *et al*. Wide-band three-dimensional submillimeter-wave holographic imaging system[J]. Journal of Terahertz Science and Electronic Information Technology(王子野,乔灵博,王迎新,等.高分辨力亚毫米波全息成像系统. **太赫兹科学与电子信息学报**)), 2016,**14**(06):833-837.

[5] Sheen D M, Bernacki B E, McMakin D L. Advanced millimeter-wave security portal imaging techniques[C]//RF and Millimeter-Wave Photonics II. International Society for Optics and Photonics, 2012, **8259**: 82590G.

[6] Ghasr M T, Horst M J, Dvorsky M R, *et al*. Wideband microwave camera for real-time 3-D imaging[J]. *IEEE Transactions on Antennas and Propagation*, 2016, **65**(1): 258-268.

[7] Sun Z, Li C, Gu S, *et al*. Fast three-dimensional image reconstruction of targets under the illumination of terahertz Gaussian beams with enhanced phase-shift migration to improve computation efficiency[J]. *IEEE Transactions on Terahertz Science and Technology*, 2014, **4**(4): 479-489.

[8] Qiao L, Wang Y, Zhao Z, *et al*. Range resolution enhancement for three-dimensional millimeter-wave holographic imaging[J]. *IEEE Antennas and Wireless Propagation Letters*, 2015, **15**: 1422-1425.

[9] Zhang Y, Deng B, Yang Q, *et al*. Near-field three-dimensional planar millimeter-wave holographic imaging by using frequency scaling algorithm[J]. *Sensors*, 2017, **17**(10): 2438.

[10] Sheen D M, McMakin D L, Lechelt W M, *et al*. Circularly polarized millimeter-wave imaging for personnel screening[C]//Passive Millimeter-Wave Imaging Technology VIII. International Society for Op-

tics and Photonics, 2005, **5789**: 117-126.

[11] Reck T, Jung-Kubiak C, Siles J V, *et al*. A silicon micromachined eight-pixel transceiver array for submillimeter-wave radar[J]. *IEEE Transactions on Terahertz Science and Technology*, 2015, **5**(2): 197-206.

[12] Ahmed S S, Schiessl A, Schmidt L P. A novel fully electronic active real-time imager based on a planar multistatic sparse array[J]. *IEEE Transactions on Microwave Theory and Techniques*, 2011, **59**(12): 3567-3576.

[13] Zhuge X, Yarovoy A G. Study on two-dimensional sparse MIMO UWB arrays for high resolution near-field imaging[J]. *IEEE transactions on antennas and propagation*, 2012, **60**(9): 4173-4182.

[14] Tan K, Wu S, Wang Y, *et al*. A novel two-dimensional sparse MIMO array topology for UWB short-range imaging[J]. *IEEE Antennas and Wireless Propagation Letters*, 2015, **15**: 702-705.

[15] Baccouche B, Agostini P, Mohammadzadeh S, *et al*. Three-dimensional terahertz imaging with sparse multistatic line arrays[J]. *IEEE Journal of Selected Topics in Quantum Electronics*, 2017, **23**(4): 1-11.

[16] Moulder W F, Krieger J D, Majewski J J, *et al*. Development of a high-throughput microwave imaging system for concealed weapons detection[C]//2016 IEEE International Symposium on Phased Array Systems and Technology (PAST). IEEE, 2016: 1-6.

[17] Gao J, Qin Y, Deng B, *et al*. Novel efficient 3D short-range imaging algorithms for a scanning 1D-MIMO array[J]. *IEEE Transactions on Image Processing*, 2018, **27**(7): 3631-3643.

[18] Gubernatis J E, Domany E, Krumhansl J A, *et al*. The Born approximation in the theory of the scattering of elastic waves by flaws[J]. *Journal of Applied Physics*, 1977, **48**(7): 2812-2819.

[19] Lopez-Sanchez J M, Fortuny-Guasch J. 3-D radar imaging using range migration techniques[J]. *IEEE Transactions on antennas and propagation*, 2000, **48**(5): 728-737.

[20] Wang Z, Guo Q, Tian X, *et al*. Near-field 3-D millimeter-wave imaging using MIMO RMA with range compensation[J]. *IEEE Transactions On Microwave Theory And Techniques*, 2018, **67**(3): 1157-1166.

[21] Evans G E. Antenna measurement techniques[J]. *Norwood*, 1990, pp. 238.

[22] Zhuge X, Yarovoy A G. A sparse aperture MIMO-SAR-based UWB imaging system for concealed weapon detection[J]. *IEEE Transactions on Geoscience and Remote Sensing*, 2010, **49**(1): 509-518.

[23] Petkie D T, Holt J A, Patrick M A, *et al*. Multimode illumination in the terahertz for elimination of target orientation requirements and minimization of coherent effects in active imaging systems[J]. *Optical Engineering*, 2012, **51**(9): 091604.